# Nonequilibrium transport of helical Luttinger liquids through a quantum dot

Sung-Po Chao,[1,2] Salman A. Silotri,[3] and Chung-Hou Chung[1,3]
[1]*Physics Division, National Center for Theoretical Science, Hsinchu, 30013, Taiwan, Republic of China*
[2]*Physics Department, National Tsing Hua University, Hsinchu, 30013, Taiwan, Republic of China*
[3]*Department of Electrophysics, National Chiao-Tung University, Hsinchu, 30010, Taiwan, Republic of China*
(Received 20 May 2013; revised manuscript received 13 July 2013; published 8 August 2013)

We study a steady-state nonequilibrium transport between two interacting helical edge states of a two-dimensional topological insulator, described by helical Luttinger liquids, through a quantum dot. For a noninteracting dot, the current is obtained analytically by including the self-energy correction to the dot's Green function. For an interacting dot, we use the equation-of-motion method to study the influence of weak on-site Coulomb interaction on the transport. We find the metal-to-insulator quantum phase transition for attractive *or* repulsive interactions in the leads when the magnitude of the interaction strength characterized by a charge sector Luttinger parameter $K$ goes beyond a critical value. The critical Luttinger parameter $K_{cr}$ depends on the hopping strengths between the dot and the leads, as well as the energy level of the dot with respect to the Fermi levels of the leads, ranging from the weak-interaction regime for the dot level off-resonance to the strong-interaction regime for the dot in resonance with the equilibrium Fermi level. Near the transition, there are various singular behaviors of current noise, dot density of state, and the decoherence rate (inverse of lifetime) of the dot, which are briefly discussed.

DOI: 10.1103/PhysRevB.88.085109 PACS number(s): 71.10.Pm, 72.10.Fk, 73.63.Kv

## I. INTRODUCTION

The topological properties of quantum matter have attracted a great deal of attention in condensed-matter systems since the discovery and comprehensive study of the quantum Hall effect. In systems with time-reversal symmetry and strong spin-orbit interactions, the quantum spin Hall insulator (QSHI) was theoretically proposed[1–3] and, soon afterwards, experimentally verified the existence of the topologically nontrivial edge states, the hallmark of QSHI, in HgTe/CdTe quantum well structures.[4,5] The QSHI is a time-reversal invariant two-dimensional electronic phase which has a bulk energy gap generated by spin-orbit interaction. The topological order[6] of this state, similar to the case of the integer quantum Hall effect, requires the presence of gapless edge states. The propagation direction at one edge is opposite for opposite spins, and thus the edge states are usually named as the helical liquids. This one-dimensional edge state is protected from elastic backscattering through time-reversal symmetry, as the backscattering requires spin flips. Recent experiments have verified the perfectly transmitted[4] Landauer conductance $2e^2/h$ as well as the spin orientations of the edge-state transport through a junction device.[5,7] There are also theoretical proposals for detecting spin orientations through a spin-polarized scanning tunneling microscope.[8]

In the presence of electron-electron interactions, these one-dimensional helical edge states form helical Luttinger liquids,[9] a new type of Luttinger liquid where the spins of electrons are tied to the directions of their momenta. This helical nature of QSHI edge states leads to various transport properties that are different from the ordinary or chiral Luttinger liquids realized as edge states of the integer quantum Hall system.

The transport properties of the helical Luttinger liquids have been discussed in the setup of a quantum point contact[10–13] between the edges. Alternatively, transport of a quantum dot[14,15] or antidot[16,17] coupled to the helical edge states offers a simple way for the detection of the helical Luttinger liquids. More interestingly, when a quantum dot is in the Kondo regime, the setup could be used to probe the transition (or crossover) between one-channel and two-channel Kondo physics[14] by changing the interaction strength or impurity concentrations of the edge state. The idea of using repulsive interaction of the electrons in the leads to suppress Kondo couplings between the two leads was suggested earlier by Fabrizio and Gogolin[18] for the case of two Luttinger liquid leads coupled to a quantum dot. They showed that the two-channel Kondo can be reached with Luttinger parameter $K < 1/2$. In the work by Law *et al.*,[14] they show that this two-channel fixed point can be reached near to equilibrium for a weaker repulsive interaction (with Luttinger parameter $K < 1$), in the context of a quantum dot coupled to two helical Luttinger liquid leads realized as edge states of the QSHI. The higher order of the renormalization group (RG) analysis[19] shows that there could be a quantum phase transition between the one-channel and two-channel Kondo in the same setup for the Luttinger parameter, $1/2 < K < 1$.

In this paper, we address a different aspect (in the resonant tunneling limit far from the Kondo regime) of the quantum dot setup in Ref. 14: we study the nonequilibrium steady-state transport problem with a noninteracting or weakly interacting quantum dot connected with two helical Luttinger liquid edges of the QSHI, as shown in Fig. 1. The problem of a noninteracting quantum dot connected to leads of chiral Luttinger liquids was studied by Chamon and Wen[20] and later generalized to the multilevel within the quantum dot by Furusaki[21] using the master-equation approach at a temperature higher than the tunneling strength. The nonequilibrium transport of a noninteracting quantum dot coupled to one side of the helical edge state and a normal Fermi-liquid lead was studied by Seng and Ng in Ref. 15. For a quantum dot connected with two edges kept at different chemical potentials, we map this problem into spinful Luttinger liquids following Hou *et al.* in Ref. 10. While helicity makes spin a redundant quantum number on a single edge,[15] it is important to include it when

 

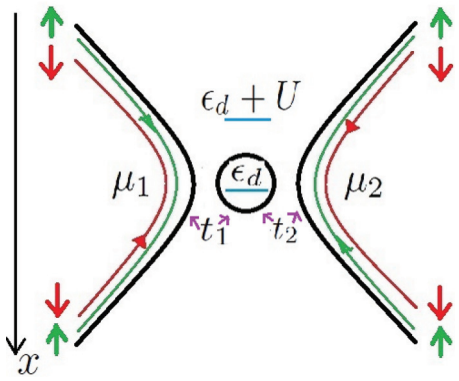


FIG. 1. (Color online) Nonequilibrium steady-state transport between two edge states of a quantum spin Hall system through a quantum dot. Dot level $\epsilon_d$ is controlled by the gate voltage applied on the quantum dot. The coupling strengths between the dot and the edge-state leads $t_1$ and $t_2$ can also be varied in the experiment. $U$ represents the on dot Coulomb interaction. The small solid green and red arrows indicates spin orientations.

two edges are connected via a quantum dot.[11] In this mapping, the charge sector Luttinger parameter $K_c$ is connected with the spin sector of Luttinger parameter $K_s$ by $K_c = 1/K_s$, a unique property owing to the helical nature of the interacting edge state of QSHI. The charge and spin susceptibility measurement[22] can be used to probe these two quantities independently and confirm their connections.

For a noninteracting dot, the dot's Green function includes all orders of perturbations via a self-energy correction with Dyson's equation, and the charge current is expressed analytically through perturbations on the Keldysh contour (Keldysh perturbation theory).[23,24] The differential conductance is obtained by numerical derivative on the current-voltage relation. We find, at zero temperature, that the zero-voltage conductance width and height decreases with increasing repulsive or attractive interactions within the edges, similar to that for other types of Luttinger liquid leads.[25,26] The equilibrium conductance reaches zero for strongly interacting edge states (with Luttinger parameter $K < 0.26$ for repulsive interaction) for the dot level on-resonance with the equilibrium Fermi surface of the edges. We compute other physical measurable quantities, such as noise[27–29] and lifetime of the dot electron, and both of them show similar transitions at the same interaction strength in the lowest-order perturbation computation. For the dot level away from the equilibrium Fermi level, this metallic-to-insulating quantum phase transition (QPT) occurs at weaker interaction strengths, as can be seen by comparing Figs. 2 and 3. Note that for very strong repulsive interactions (when the Luttinger parameter $K < 1/4$), random two-particle backscatterings, albeit preserving time-reversal symmetry, destabilize the edge states.[30,31] Magnetic impurities along the edge also destabilize the edge states[32] for $K < 1/4$. This hinders the possibility of observing the QPT in experiment if the dot level is at resonance with the equilibrium Fermi sea, but we shall be able to observe this QPT by tuning the dot level off-resonance. *The dot level, controlled by the gate voltage upon it, serves as another tunable parameter, in addition to interaction strengths of the edge states, to drive this QPT.*

For a weakly interacting dot, we use the equation-of-motion approach to compute perturbatively the influence of Coulomb repulsion for double occupancy on the quantum dot. For the dot level at resonance, we again find the metal-to-insulator transition at the same critical interaction strength, $K_{cr} \sim 0.26$, as that for a noninteracting dot.

This paper is organized as follows. In Sec. II, we set up the model Hamiltonian and apply bosonization[22,33] to solve for the edge-state Hamiltonian before coupling it to the quantum dot. In the presence of a quantum dot, we use Keldysh perturbation theory to compute the charge current through the quantum dot. The calculations for the noninteracting dot on the current, noise through the quantum dot, and the lifetime of the dot electron are summarized in Sec. III. In Sec. IV, we compute the current transport through a weakly interacting dot. The last section is devoted to the conclusion. Derivations of various correlators of the edge states are shown in the Appendix.

## II. MODEL HAMILTONIAN

Following Hou *et al.* in Ref. 10, we model the two edge states of the QSHI kept at chemical potentials $\mu_1$ and $\mu_2$ connected via a quantum dot as

$$
\begin{aligned}
H &= H_{\text{edges}} + H_{\text{dot}} + H_{\text{int}} = H_0 + H_{\text{int}},\\
H_{\text{edges}} &= \int dx \Bigg( \sum_\sigma \{ i v_F [\psi^\dagger_{L\sigma}(x)\partial\psi_{L\sigma}(x) - \psi^\dagger_{R\sigma}(x)\partial\psi_{R\sigma}(x)] + u_2 \psi^\dagger_{L\sigma}(x)\psi_{L\sigma}(x)\psi^\dagger_{R-\sigma}(x)\psi_{R-\sigma}(x)\\
&\quad + \frac{u_4}{2}[\psi^\dagger_{L\sigma}(x)\psi_{L\sigma}(x)\psi^\dagger_{L\sigma}(x)\psi_{L\sigma}(x) + \psi^\dagger_{R\sigma}(x)\psi_{R\sigma}(x)\psi^\dagger_{R\sigma}(x)\psi_{R\sigma}(x)]\}\\
&\quad - \mu_1[\psi^\dagger_{R\uparrow}(x)\psi_{R\uparrow}(x) + \psi^\dagger_{L\downarrow}(x)\psi_{L\downarrow}(x)] - \mu_2\big[\psi^\dagger_{L\uparrow}(x)\psi_{L\uparrow}(x) + \psi^\dagger_{R\downarrow}(x)\psi_{R\downarrow}(x)\big] \Bigg), \qquad (1)\\
H_{\text{dot}} &= \sum_\sigma \epsilon_d d^\dagger_\sigma d_\sigma + U d^\dagger_\uparrow d_\uparrow d^\dagger_\downarrow d_\downarrow,\\
H_{\text{int}} &= \{ t_1[\psi^\dagger_{R\uparrow}(0)d_\uparrow + \psi^\dagger_{L\downarrow}(0)d_\downarrow + \text{H.c.}] + t_2[\psi^\dagger_{L\uparrow}(0)d_\uparrow + \psi^\dagger_{R\downarrow}(0)d_\downarrow + \text{H.c.}]\}.
\end{aligned}
$$

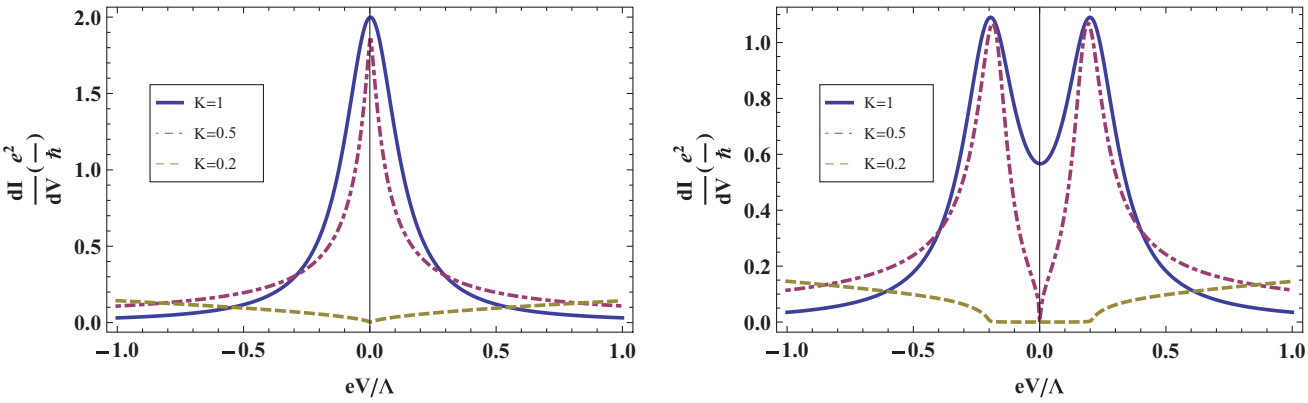


FIG. 2. (Color online) Differential conductance as a function of voltage obtained numerically for $K = 1$ (blue line), $K = 0.5$ (purple dot-dashed line), $K = 0.2$ (brown dashed line), and $t/\Lambda = 0.1$. Left: $\epsilon_d/\Lambda = 0$. Right: $\epsilon_d/\Lambda = -0.1$. Note that the insulating behavior at $V = 0$ occurs at larger $K$ value (for repulsive interaction, the $K = 0.5$ is already in the insulating phase at zero voltage) compared with the $\epsilon_d = 0$ case.

Here $u_2$, $u_4$ are the interaction constants modeling the short-range interaction within the edge. $\epsilon_d$ is the dot energy level and $U$ is the on dot Coulomb interaction. $t_1$ and $t_2$ are the coupling strengths between the edges and the dot. We use the spinful bosonization by writing the fermion fields of the edge states as

$$\psi_{L\sigma}(x) = \frac{1}{\sqrt{2\pi a_0}}\eta_\sigma e^{-i\sqrt{4\pi}\phi_{L\sigma}(x)},$$
$$\psi_{R\sigma}(x) = \frac{1}{\sqrt{2\pi a_0}}\eta_\sigma e^{-i\sqrt{4\pi}\phi_{R\sigma}(x)},$$

with $\eta_\sigma$ as the Klein factor chosen to satisfy the fermion anticommutation rule and $a_0$ as the lattice cutoff for the linear spectrum. Define the bosonic fields

$$\Phi_\sigma/\Theta_\sigma = \phi_{L\sigma} \pm \phi_{R\sigma}$$

and denote their charge and spin sectors as

$$\Phi_c = \frac{1}{\sqrt{2}}(\Phi_\uparrow + \Phi_\downarrow), \quad \Phi_s = \frac{1}{\sqrt{2}}(\Phi_\uparrow - \Phi_\downarrow),$$

and the similar expressions for $\Theta_c$ and $\Theta_s$. We choose a time-dependent gauge transformation to move the chemical potentials in $H_0$ to $H_{\rm int}$ by writing

$$\psi_{R\uparrow}/\psi_{L\downarrow} \to e^{i\mu_1 t}\psi_{R\uparrow}/\psi_{L\downarrow},$$
$$\psi_{L\uparrow}/\psi_{R\downarrow} \to e^{i\mu_2 t}\psi_{L\uparrow}/\psi_{R\downarrow}.$$

With these transformations, we rewrite Eq. (1) as

$$H_0 = \sum_{\alpha=c,s}\frac{v_\alpha}{2}\int_{-\infty}^{\infty}dx : \left[K_\alpha(\partial_x\Theta_\alpha)^2 + \frac{1}{K_\alpha}(\partial_x\Phi_\alpha)^2\right] :$$
$$+ \sum_\sigma \epsilon_d d_\sigma^\dagger d_\sigma + U d_\uparrow^\dagger d_\uparrow d_\downarrow^\dagger d_\downarrow,$$
$$H_{\rm int} = \sum_\sigma (t_{R\sigma}e^{-i\mu_{R\sigma}t - i\sqrt{4\pi}\phi_{R\sigma}(0)}\eta_{R\sigma}^\dagger d_\sigma$$
$$+ t_{L\sigma}e^{-i\mu_{L\sigma}t - i\sqrt{4\pi}\phi_{L\sigma}(0)}\eta_{L\sigma}^\dagger d_\sigma + \text{H.c.}), \qquad (2)$$

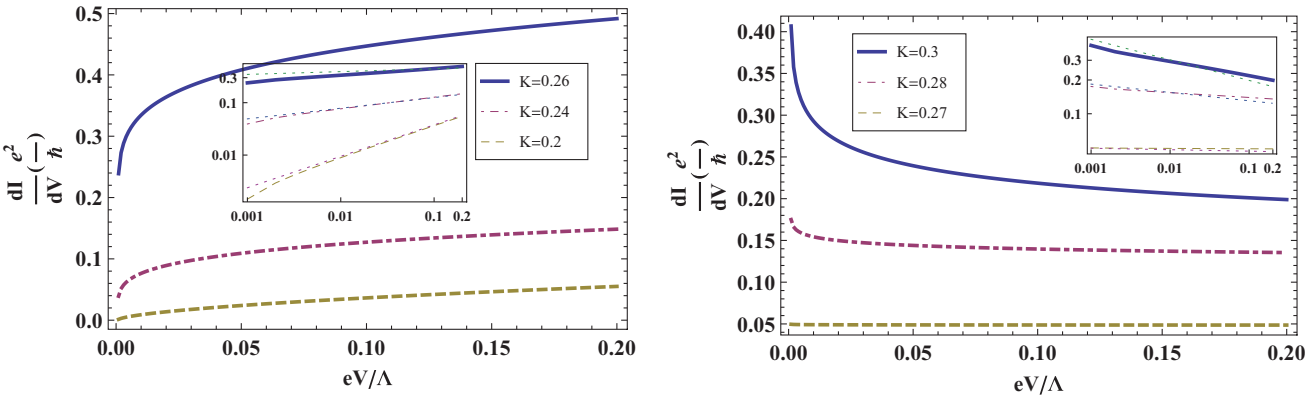


FIG. 3. (Color online) $dI/dV$ vs $V$ for various interaction strengths with $t/\Lambda = 0.1$, $\epsilon_d = 0$, and $\mu_1 = -\mu_2 = \frac{eV}{2}$. The inset shows a double logarithmic plot, illustrating the power-law behavior for conductance ($dI/dV \propto V^{\frac{1}{2}(K+\frac{1}{K})-2}$) slightly away from the resonance value, $eV \simeq \epsilon_d$. Deviations near resonance can be accounted for by a higher-order RG. The straight dotted lines are generated for guidance by functions proportional to $V^{\frac{1}{2}(K+\frac{1}{K})-2}$ for different Luttinger parameter $K$. Left: Insulating phase for $K \leqslant K_{cr} \sim 0.267$: $K = 0.26$ (blue line), $K = 0.24$ (purple dot-dashed line), $K = 0.2$ (brown dashed line). Right: Conducting phase for $K \geqslant K_{cr}$: $K = 0.3$ (blue line), $K = 0.28$ (purple dot-dashed line), $K = 0.27$ (brown dashed line).

with $K_c = 1/K_s = K = \sqrt{\frac{1+\frac{u_4}{2\pi v_F}-\frac{u_2}{2\pi v_F}}{1+\frac{u_4}{2\pi v_F}+\frac{u_2}{2\pi v_F}}}$, $v_c = v_s = v = v_F\sqrt{(1+\frac{u_4}{2\pi v_F})^2-(\frac{u_2}{2\pi v_F})^2}$, $t_{R\uparrow} = t_{L\downarrow} = t_1/\sqrt{2\pi a_0}$, $t_{L\uparrow} = t_{R\downarrow} = t_2/\sqrt{2\pi a_0}$, $\mu_{R\uparrow} = \mu_{L\downarrow} = \mu_1$, and $\mu_{L\uparrow} = \mu_{R\downarrow} = \mu_2$. For repulsive interaction in the edge states, $u_2 > 0$ and $u_4 > 0$, which leads to Luttinger parameter $K < 1$. For attractive interaction, we have Luttinger parameter $K > 1$. The particle current at time $t$, or $I_1(t)/e = -I_2(t)/e$ with $e$ as electric charge, is obtained by the Heisenberg equation:

$$\begin{aligned} I_1(t)/e &= d\langle\psi^\dagger_{R\uparrow}(0)\psi_{R\uparrow}(0)+\psi^\dagger_{L\downarrow}(0)\psi_{L\downarrow}(0)\rangle/dt \\ &= -i\langle[\psi^\dagger_{R\uparrow}(0)\psi_{R\uparrow}(0)+\psi^\dagger_{L\downarrow}(0)\psi_{L\downarrow}(0),H]\rangle \\ &= 2t_1\mathrm{Im}[\langle e^{-i\mu_{R\uparrow}t}\psi^\dagger_{R\uparrow}(0)d_\uparrow + e^{-i\mu_{L\downarrow}t}\psi^\dagger_{L\downarrow}(0)d_\downarrow\rangle] \\ &= 2\mathrm{Im}[\langle t_{R\uparrow}e^{-i\sqrt{4\pi}\phi_{R\uparrow}(0,t)}\eta^\dagger_{R\uparrow}d_\uparrow \\ &\quad + t_{L\downarrow}e^{-i\sqrt{4\pi}\phi_{L\downarrow}(0,t)}\eta^\dagger_{L\downarrow}d_\downarrow\rangle]. \end{aligned}$$

Here, $\phi_{R/L\sigma}(0,t) \equiv \phi_{R/L\sigma}(0) + \mu_{R/L\sigma}t/\sqrt{4\pi}$. By defining the Keldysh contour ordered Green function $G_{\sigma,R/L\sigma}(t,t') = -i\langle T_c\{d_\sigma(t)\psi^\dagger_{R/L\sigma}(t')\}\rangle$, we express the particle current as

$$\begin{aligned} I(t)/e &= [I_1(t)-I_2(t)]/2e \\ &= \mathrm{Re}\left[\sum_{j=R,L;\sigma}(-1)^{j\sigma}t_{j\sigma}e^{-i\mu_{j\sigma}t}G^<_{\sigma,j\sigma}(t,t)\right]. \end{aligned} \quad (3)$$

The sign $(-1)^{j\sigma}$ is chosen as $(-1)^{L\uparrow} = (-1)^{R\downarrow} = -1$ and $(-1)^{R\uparrow} = (-1)^{L\downarrow} = 1$. This lesser mixed Green function $G^<_{\sigma,j\sigma}(t,t)$ is obtained by analytic continuation of contour ordered Green function $G_{\sigma,R/L\sigma}(\tau,\tau')$ in imaginary time $\tau$ and $\tau'$, with its expression given by perturbation as

$$\begin{aligned} G_{\sigma,R/L\sigma}(\tau,\tau') = \sum_{l=0}^{\infty}\frac{(-i)^{l+1}}{l!}\int_c d\tau_1\cdots\int_c d\tau_l\langle T_c\{d_\sigma(\tau) \\ \times H_{\mathrm{int}}(\tau_1)\cdots H_{\mathrm{int}}(\tau_l)\psi^\dagger_{R/L\sigma}(\tau')\}\rangle. \end{aligned} \quad (4)$$

In applying the Wick theorem in Eq. (4), we should also include all possible four fermion interaction terms ($u_2$ and $u_4$ terms in the edge-state Hamiltonian) between any two fermion operators. We use the spinful bosonization as a way to sum up all orders of perturbation in the four fermion interactions in Keldysh form. The edge-state correlators evaluated this way are thus fully dressed in our treatment and we do not specify this aspect in the expression of Eq. (4).

In the following two sections, we solve this mixed Green function perturbatively in the case of a noninteracting dot and use the equation-of-motion approach to study the case of a weak on dot interaction $U$ at zero temperature.

## III. NONINTERACTING DOT

### A. Charge current

For a noninteracting quantum dot ($U = 0$), the $H_0$ is quadratic in the dot electron operator $d_\sigma$ and the lowest nonzero perturbation gives

$$G_{\sigma,R/L\sigma}(\tau,\tau') = -\int_c d\tau_1\langle T_c\{d_\sigma(\tau)H_{\mathrm{int}}(\tau_1)\psi^\dagger_{R/L\sigma}(\tau')\}\rangle,$$

which involves a bare dot Green function, $iG^{(0)}_{d_\sigma}(\tau,\tau_1) = \langle T_c\{d_\sigma(\tau)d^\dagger_\sigma(\tau_1)\}\rangle$, and bare edge-state Green function, $iG_{\psi_{R/L,\sigma}}(\tau,\tau_1) = \langle T_c\{\psi_{R/L\sigma}(\tau_1)\psi^\dagger_{R/L\sigma}(\tau')e^{-i\mu_{R/L\sigma}(\tau'-\tau_1)}\}\rangle$. The terminology "bare" here means that the dot and leads are decoupled. The decoupled leads or edge states are described by fully interacting helical Luttinger liquids. From Eq. (4), we sum over all orders of $H_{\mathrm{int}}$ and the Fourier transformed full retarded dot Green function is given by

$$G^R_{d\sigma}(\omega) = G^{(0)R}_{d\sigma}(\omega) + G^{(0)R}_{d\sigma}(\omega)\Sigma^R_\sigma(\omega)G^R_{d\sigma}(\omega).$$

Similarly, the full dot lesser Green function is $G^<_{d\sigma}(\omega) = G^R_{d\sigma}(\omega)\Sigma^<_\sigma(\omega)G^A_{d\sigma}(\omega)$. Here the dot self-energy is

$$\Sigma_\sigma(\omega) \equiv \sum_j |t_{j\sigma}|^2 G_{\psi_j,\sigma}(\omega). \quad (5)$$

The bare dot retarded Green function is $G^{(0)R}_{d\sigma}(\omega) = 1/(w - \epsilon_d + i0^+)$. The charge current is

$$\begin{aligned} I(t) &= e\mathrm{Re}\left[\sum_{j=R,L;\sigma}(-1)^{j\sigma}t_{j\sigma}e^{-i\mu_{\alpha\sigma}t}G^<_{\sigma,j\sigma}(t,t)\right] \\ &= e\mathrm{Re}\left\{\sum_{j,\sigma}(-1)^{j\sigma}|t_{j\sigma}|^2\int dt_1\big[G^R_{d_\sigma}(t,t_1)G^<_{\psi_{j,\sigma}}(t_1,t) \right. \\ &\quad \left. + G^<_{d_\sigma}(t,t_1)G^A_{\psi_{j,\sigma}}(t_1,t)\big]\right\}. \end{aligned} \quad (6)$$

For the steady state, $G_{\psi_{j,\sigma}}(t,t_1) = G_{\psi_{j,\sigma}}(t-t_1)$ and $G_{d_\sigma}(t,t_1) = G_{d_\sigma}(t-t_1)$. We rewrite the steady-state current $I(t) = \langle\hat{I}\rangle$ as

$$\begin{aligned} \langle\hat{I}\rangle &= e\mathrm{Re}\left\{\sum_{j,\sigma}(-1)^{j\sigma}|t_{j\sigma}|^2\int d\omega\big[G^R_{d_\sigma}(\omega)G^<_{\psi_{j,\sigma}}(\omega) \right. \\ &\quad \left. + G^<_{d_\sigma}(\omega)G^A_{\psi_{j,\sigma}}(\omega)\big]\right\}. \end{aligned} \quad (7)$$

The various $G_{\psi_{j,\sigma}}(\omega)$ are computed in the Appendix and we use them to obtain the full dot Green function. The current at zero temperature is evaluated numerically and the differential conductance, obtained by taking the numerical derivative on the current-voltage curves, for symmetrically coupled ($t_1 = t_2$) and symmetrically driven voltage ($\mu_1 = -\mu_2 = eV/2$) is plotted in the left figure of Fig. 2 for the $\epsilon_d = 0$ case and is plotted in the right figure of Fig. 2 for $\epsilon_d = -0.1\Lambda$. For asymmetrically driven voltage or $t_1 \neq t_2$, the overall features discussed below are similar, but the symmetry between positive and negative voltage breaks. Thus we concentrate on the case for $t_1 = t_2$ and $\mu_1 = -\mu_2$ in our analysis hereafter. For $\epsilon_d = 0$, with 0 as our equilibrium Fermi level, the scaling dimension obtained from the zeroth-order RG analysis[33] in $H_{\mathrm{int}}$ is $(K_c + K_s + 1/K_c + 1/K_s)/8$, which renders the

renormalized coupling $t$ in equilibrium as

$$\frac{dt}{d\ln(\Lambda)} = \left(1 - \frac{K_c + K_s + 1/K_c + 1/K_s}{8}\right)t, \qquad (8)$$

with $\Lambda = \hbar v/a_0$ as the UV cutoff for the linear spectrum of the edge states. For the quantum spin Hall state, $K_c = 1/K_s = K$ and we have the critical value of $K_{cr} = 2 \pm \sqrt{3}$. That is, for $0.267 < K < 3.733$, we have finite conductance at $V = 0$ and insulating behavior for $K < 0.26$ or $K > 3.733$. To understand this critical behavior for the dot level in resonance with the equilibrium Fermi surface, we plot the differential conductance versus source drain voltage in Fig. 3 for Luttinger parameter $K$ chosen slightly below (left figure of Fig. 3) and above (right figure of Fig. 3) the critical Luttinger parameter $K_{cr} = 2 \pm \sqrt{3}$. The inset shows the double logarithm plots for both figures and, in both cases, shows $dI/dV \propto V^{\frac{1}{2}(K+\frac{1}{K})-2}$ for voltage slightly off-resonance. The drastic difference near $V \simeq 0$ clearly illustrates the metal-to-insulator transition across the critical Luttinger parameter, $K_{cr} \sim 0.26$, for the dot level in resonance with the equilibrium Fermi level.

Note that although the hopping term $t$ here is relevant (at the tree level) in the metallic phase with a scaling dimension $[t] = (K_c + K_s + 1/K_c + 1/K_s)/8 < 1$ [see Eq. (8)], our perturbative calculation for $U = 0$ is still controlled as the hopping term is treated exactly due to the quadratic nature of our Hamiltonian in terms of the impurity (dot) operator $d_\sigma$. A similar property can be found in other systems, including the noninteracting single impurity Anderson model[34] and the noninteracting pseudogap Anderson model.[35]

For $\epsilon_d \neq 0$, i.e., the dot level away from the equilibrium Fermi level of the two leads, as shown in the right figure of Fig. 2, the transition occurs at a larger $K$ value for $0 < K < 1$ (say, showing insulating behavior at $K = 0.5$ for $\epsilon_d/\Lambda = -0.1$ and $t/\Lambda = 0.1$, shown as a purple dot-dashed line), indicating that a smaller repulsive interaction within the edge states would lead to the insulating phase in this off-resonance regime near equilibrium. When the dot level is far from the edge potentials, we can carry out an off-resonance study by integrating out the dot electron state,[20] obtaining an effective single-particle hopping term,

$$H_{\rm int} \sim \frac{t_1 t_2^\dagger}{|\epsilon_d - \mu|}[\psi_{R\uparrow}(0)^\dagger \psi_{L\uparrow}(0) + \psi_{L\downarrow}(0)^\dagger \psi_{R\downarrow}(0)] + \text{H.c.} \qquad (9)$$

Here, $\mu = (\mu_1 + \mu_2)/2$ is the equilibrium Fermi level of the edge states and the projection is done assuming $eV = |\mu_1 - \mu_2| \ll |\epsilon_d - \mu|$. This single-particle tunneling current, as well as the current noise associated with it, has been analyzed by Lee *et al.* in Ref. 29. For $t = t_1 = t_2$, the single-particle tunneling current[29] $I_t$ at zero temperature is

$$I_t \propto \frac{e|t|^2}{|\epsilon_d - \mu|} V^{K+\frac{1}{K}-1}, \qquad (10)$$

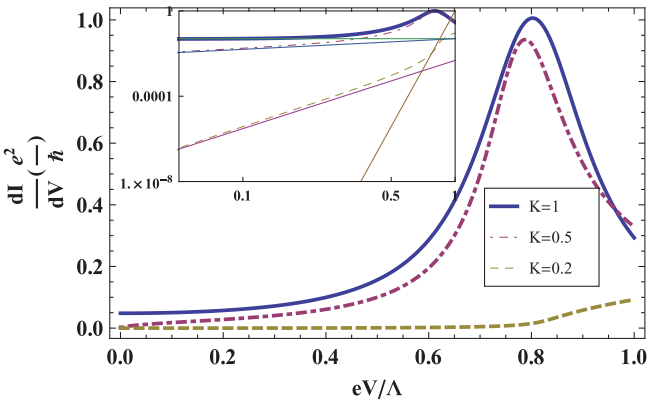


FIG. 4. (Color online) Differential conductance as a function of voltage obtained numerically for $K = 1$ (blue line), $K = 0.5$ (purple dot-dashed line), and $K = 0.2$ (brown dashed line). $\epsilon_d/\Lambda = -0.4$, $t/\Lambda = 0.1$, and $\mu_1 = -\mu_2 = eV/2$. The inset shows the double logarithmic plot with the top three thin straight lines attached to the numerical data away from the resonance peak, generated for guidance by functions proportional to $V^{(K+\frac{1}{K})-2}$ for the corresponding different Luttinger parameter $K$. The steepest (brown) thin straight line corresponds to the two-particle scattering process generated by the function proportional to $V^{(\frac{4}{K}-2)}$ for the $K = 0.2$ case. A small region close to the resonance peak is described by this power-law behavior.

which renders single-particle tunneling conductance $dI_t/dV \propto V^{K+\frac{1}{K}-2}$ and the insulating phases occur at $K \neq 1$. Thus, for the off-resonance case, any nonzero interaction strength, attractive or repulsive, would lead to the insulating phase at zero bias. The power-law behavior in Eq. (10) is consistent with our numerical results for the off-resonance case shown in Fig. 4. The inset of Fig. 4 shows that a large portion of the conductance is indeed proportional to $V^{K+\frac{1}{K}-2}$. The upturn close to the resonance could be taken into account by including multiparticle tunneling events, as considered by Kane and Fisher in Ref. 26 for the two-particle tunneling process in the chiral Luttinger liquids, or by Teo and Kane in Ref. 12 in the helical Luttinger liquids. The multiparticle tunneling events are a natural result from our analysis as we include all orders of perturbation through the dot self-energy term. For example, the two-particle tunneling process[12,26,29] gives $dI_t/dV \propto V^{(\frac{4}{K}-2)}$, which is illustrated in the steepest dotted line in the inset of Fig. 4 for the $K = 0.2$ case. The critical Luttinger parameter for the two-particle tunneling is obtained by the zero of the power in differential conductance which renders $K_{cr} = 2$. The other critical value, $K_{cr} = 1/2$, corresponds to the conducting-insulating transition for spin current,[10,12] which cannot be observed in this charge current analysis.

The fact that multiparticle tunneling processes show up near the resonance peak is understood as follows. Due to the higher power in the small parameter $t/|\epsilon_d - \mu|$ in perturbative expansion with the dot Green function, the multiparticle tunneling process amplitude is diminishingly small for the dot level $\epsilon_d$ away from the Fermi levels. Higher-order terms become more important when $\epsilon_d$ is closer to one of the chemical potentials in the nonequilibrium regime.

### B. Current noise and lifetime of dot electron

Similar to the chiral Luttinger liquids,[20] the metal-insulator transition driven by interaction within the helical Luttinger edge states can also be probed in the noise[27–29] or phase-sensitive measurement. The noise spectrum is given by the current-current correlation $S(V,\omega) = \int dt e^{i\omega t}\langle\{\Delta\hat{I}(t),\Delta\hat{I}(0)\}\rangle$. At zero temperature, the lowest-order perturbation of $S(V,\omega)$ is proportional to the Fourier transform of $\langle\{\hat{I}(t),\hat{I}(0)\}\rangle$, which is expressed as

$$\langle\{\hat{I}(t),\hat{I}(0)\}\rangle \propto \sum_{\sigma} |t_1|^2\langle e^{-i\mu_1 t}\psi^{\dagger}_{1\sigma}(t)d_{\sigma}(t)d^{\dagger}_{\sigma}(0)\psi_{1\sigma}(0) + e^{i\mu_1 t}d^{\dagger}_{\sigma}(t)\psi_{1\sigma}(t)\psi^{\dagger}_{1\sigma}(0)d_{\sigma}(0)\rangle + |t_2|^2\langle e^{-i\mu_2 t}\psi^{\dagger}_{2\sigma}(t)d_{\sigma}(t) \times d^{\dagger}_{\sigma}(0)\psi_{2\sigma}(0) + e^{i\mu_2 t}d^{\dagger}_{\sigma}(t)\psi_{2\sigma}(t)\psi^{\dagger}_{2\sigma}(0)d_{\sigma}(0)\rangle. \quad (11)$$

The zeroth-order dot electron correlator in the time domain is given by $\langle d^{\dagger}_{\sigma}(t)d_{\sigma}(0)\rangle = \theta(\epsilon_d)e^{-i\epsilon_d t}$ at zero temperature. Thus, the lowest-order $S(V,\omega)$ is

$$S(V,\omega) \simeq \frac{2\pi e^2}{\Gamma(4\kappa)}\left(\frac{a_0}{v}\right)^{4\kappa}(|t_1|^2\{|\omega-\mu_1+\epsilon_d|^{4\kappa-1}\theta(\omega-\mu_1+\epsilon_d) + |\omega+\mu_1-\epsilon_d|^{4\kappa-1}\theta[-(\omega+\mu_1-\epsilon_d)]\} + |t_2|^2\{|\omega-\mu_2+\epsilon_d|^{4\kappa-1}\theta(\omega-\mu_2+\epsilon_d) + |\omega+\mu_2-\epsilon_d|^{4\kappa-1}\theta[-(\omega+\mu_2-\epsilon_d)]\}). \quad (12)$$

Here, $\kappa = \frac{1}{8}(K+\frac{1}{K})$. For the lowest-order perturbation, $S(V,0) = ev\langle\hat{I}\rangle_0$, with $\langle\hat{I}\rangle_0$ denoting the lowest-order current. The zero-frequency noise as a function of voltage and fixed voltage noise as a function of frequency are plotted in the left and right figures of Fig. 5. From the left figure, we see there is a discontinuity that occurs at voltage $|eV/2| \sim |\epsilon_d|$ for $0.26 < K < 1$ (the discontinuity is not easy to see for $K < 0.5$ in Fig. 5) and a continuous curve for $0 < K < 0.26$ for the repulsive interaction. This transition happens at the same critical value of the Luttinger parameter for the dot level in resonance with the equilibrium Fermi level. The discontinuity is easier to identify by looking at its first derivative $\partial S(V,0)/\partial V$, which is proportional to differential conductance $dI/dV$ at the lowest-order perturbation. The divergence at $|eV/2| \sim |\epsilon_d|$ for $\partial S(V,0)/\partial V \propto |eV/2-\epsilon_d|^{4\kappa-2}$ for $\kappa < 1/2$, equivalent to $0.26 < K < 1$ in the repulsive regime, indicates the discontinuity. Similar discontinuities are also found in the fixed voltage noise where $\partial S(V,\omega)/\partial\omega$ shows discontinuities at $\omega \sim |eV/2 \pm \epsilon_d|$ for $0.26 < K < 1$.

The phase-sensitive measurement, such as the Aharonov-Bohm ring measurement, gives the information of the dot lifetime defined as $-\mathrm{Im}[\Sigma^R_{\sigma}(V,\omega)]$. Following the Appendix with symmetric coupling $t_1 = t_2$, we have

$$-\mathrm{Im}\left[\Sigma^R_{\sigma}(V,\omega)\right] \propto (|\omega-\mu_1|^{4\kappa-1} + |\omega-\mu_2|^{4\kappa-1}). \quad (13)$$

As Eq. (13) shares a similar power-law behavior as Eq. (12) for the $\epsilon_d = 0$ case, they show similar discontinuity behaviors. The lifetimes for fixed voltage or fixed frequency are plotted in Fig. 6. For fixed voltage (left figure), we see again the dips structure at $\omega \sim \pm eV/2$, which is a symmetric function of frequency as we choose symmetrical couplings. For zero frequency, we see discontinuity at $V \sim 0$ for $0.26 < K < 1$ in the repulsive case.

## IV. WEAKLY INTERACTING DOT

For small $U$, we use the equation-of-motion method to obtain the dot Green function without coupling to the edge states. Then we take the interacting isolated dot Green function as the unperturbed dot Green function and add the self-energy term in Eq. (5) as the approximated dressed dot Green function. This method is equivalent to making the

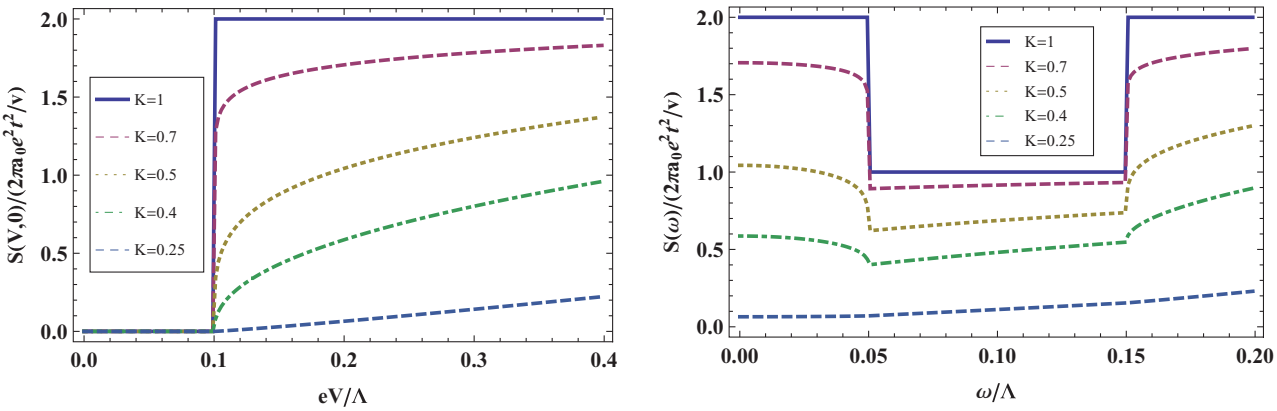


FIG. 5. (Color online) Noise for different Luttinger parameters $K = 1$ (blue line), $K = 0.7$ (purple dashed line), $K = 0.5$ (brown dotted line), $K = 0.4$ (green dot-dashed line), $K = 0.25$ (light-blue dashed line), and $\epsilon_d/\Lambda = -0.05$ in both figures. Left: Zero-frequency noise $S(V,0)$ as a function of voltage. Right: $S(V,\omega)$ for fixed voltage with $eV/2\Lambda = 0.1$ as a function of frequency.

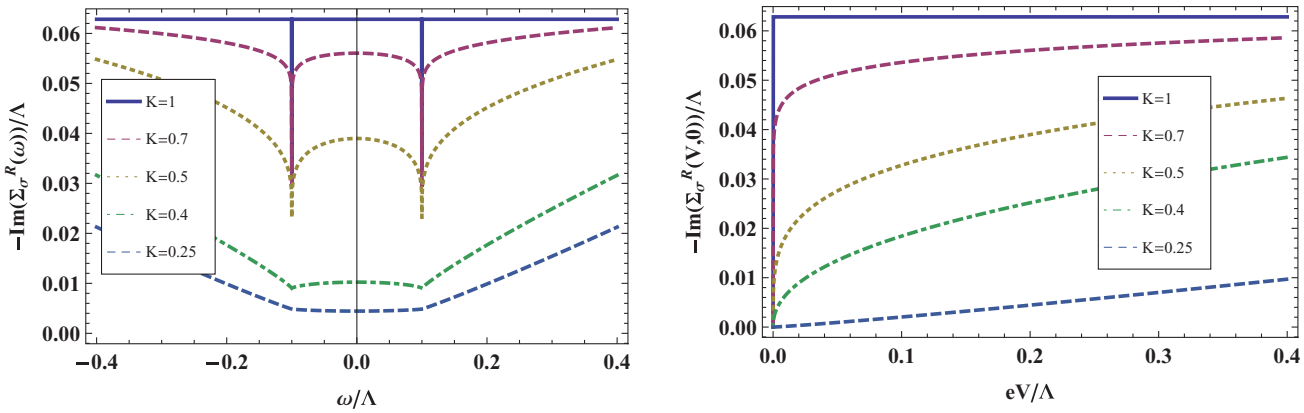


FIG. 6. (Color online) Lifetime for different Luttinger parameters $K = 1$ (blue line), $K = 0.7$ (purple dashed line), $K = 0.5$ (brown dotted line), $K = 0.4$ (green dot-dashed line), $K = 0.25$ (light-blue dashed line), and $t/\Lambda = 0.1$ in both cases. Left: Lifetime for $|eV/\Lambda| = 0.2$ as a function of frequency. Right: Lifetime for $\omega = 0$ as a function of voltage.

Hartree-Fock approximation[24] to the higher-order correlation generated in the equation-of-motion approach with the dot coupled to the edge states. Our approach, which is equivalent to that in Ref. 34 for the single impurity Anderson model in the presence of weak on-site Coulomb interaction on the impurity ($U/t \ll 1$), is described as follows.

The retarded Green function of the isolated dot is

$$g^R_{\sigma\sigma}(t) = -i\theta(t)\langle\{d_\sigma(t), d^\dagger_\sigma(0)\}\rangle.$$

By taking the time derivative and use the Heisenberg equation of motion $i\dot{d}_\sigma = \epsilon_d d_\sigma + U[d_\sigma, n_\sigma n_{\bar\sigma}] = \epsilon_d d_\sigma + U d_\sigma n_{\bar\sigma}$ to replace $\dot{d}_\sigma$, we obtain

$$i\frac{\partial g^R_{\sigma\sigma}(t)}{\partial t} = \delta(t) + \epsilon_d g^R_{\sigma\sigma}(t) + U g_{\sigma\bar\sigma}(t). \tag{14}$$

In Eq. (14), we define the two-particle correlator, $-i\theta(t)\langle\{d_\sigma(t)n_{\bar\sigma}(t), d^\dagger_\sigma(0)\}\rangle \equiv g_{\sigma\bar\sigma}(t)$. By taking the time derivative on $g_{\sigma\bar\sigma}(t)$, we get

$$i\frac{\partial g_{\sigma\bar\sigma}(t)}{\partial t} = \delta(t)\langle n_{\bar\sigma}\rangle + \epsilon_d g_{\sigma\bar\sigma}(t) + U g_{\sigma\bar\sigma}(t). \tag{15}$$

By combining Eqs. (14) and (15) and taking the Fourier transform, we obtain

$$g^R_{\sigma\sigma}(\omega) = \frac{\langle n_{\bar\sigma}\rangle}{\omega - \epsilon_d - U + i\delta} + \frac{1 - \langle n_{\bar\sigma}\rangle}{\omega - \epsilon_d + i\delta}. \tag{16}$$

The interacting dot Green function connected to the edge states is approximated by

$$G^R_{\sigma\sigma}(\omega) \simeq \frac{1}{\left[g^R_{\sigma\sigma}(\omega)\right]^{-1} - \Sigma^R_\sigma(\omega)}, \tag{17}$$

with the self-energy given by Eq. (5). The $\langle n_{\bar\sigma}\rangle$ in Eq. (16) is obtained self-consistently through numerical iterations by

$$\langle n_{\bar\sigma}\rangle = \int \frac{d\omega}{2\pi i} G^<_{\bar\sigma\bar\sigma}(\omega). \tag{18}$$

Here, $G^<_{\bar\sigma\bar\sigma}(\omega) = G^R_{\bar\sigma\bar\sigma}(\omega)\Sigma^<_{\bar\sigma}(\omega)G^A_{\bar\sigma\bar\sigma}(\omega)$. The differential conductance is obtained by taking the numerical derivative on the current, and the result for different interaction strengths within the edge states is shown in Fig. 7.

From Fig. 7, the metal-insulator transition near equilibrium occurs at the Luttinger parameter $K \simeq 0.26$, which is the same as the noninteracting dot case. The positions of the side peaks are at $\mu_1/\mu_2 \sim \epsilon_d + U$ ($|eV/\Lambda| \sim 0.2$ in Fig. 7) as a result of the charge fluctuations on the dot. These charge fluctuation side peaks become dips as the Luttinger parameter $K < 0.26$ and the overall magnitude as well as the

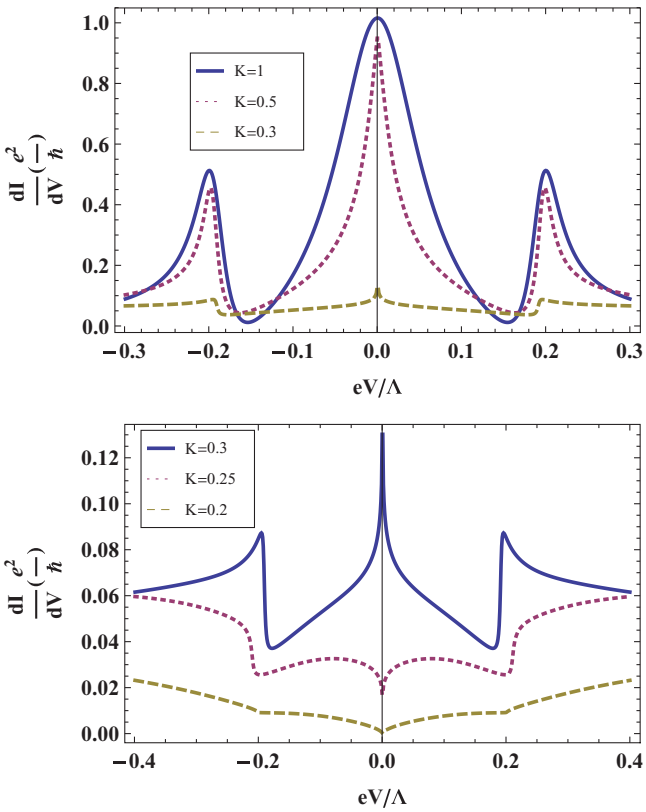


FIG. 7. (Color online) Differential conductance vs source drain voltage for $t/\Lambda = 0.075$, $\epsilon_d = 0$, $U/\Lambda = 0.1$, and $\mu_1 = -\mu_2 = eV/2$ with different interaction strengths within the edge states. Top: $K = 1$ (blue solid line), $K = 0.5$ (purple dotted line), $K = 0.3$ (brown dashed line). Bottom: $K = 0.3$ (blue solid line), $K = 0.25$ (purple dotted line), $K = 0.2$ (brown dashed line).

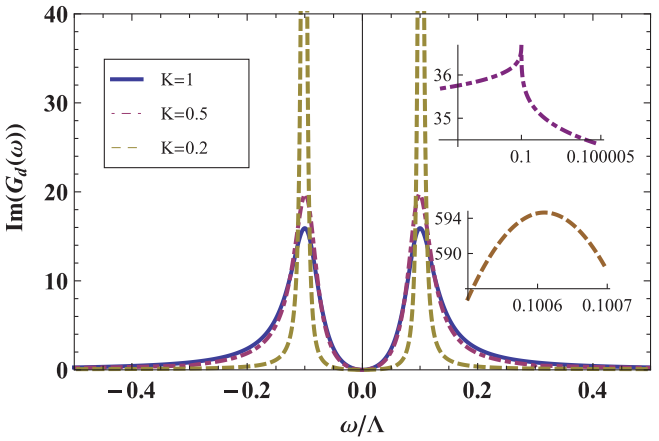


FIG. 8. (Color online) Imaginary part of the nonequilibrium steady-state dot Green function for $t/\Lambda = 0.1$, $\epsilon_d/\Lambda = -U/2\Lambda = -0.1$, and $\mu_1 = -\mu_2 = eV/2 = 0.1\Lambda$ with different interaction strengths within the edge states: $K = 1$ (blue solid line), $K = 0.5$ (purple dot-dashed line), and $K = 0.2$ (brown dashed line). The inset shows the blowup of $K = 0.5$ (upper inset) and $K = 0.2$ (lower inset) cases for regions $\omega \simeq |eV/2|$. The singular behavior for $0.26 < K < 1$ for the repulsive interaction has the same root as the singular behavior in the dot lifetime, $-\mathrm{Im}[\Sigma^R_\sigma(\omega)]$.

width of the resonance peaks decreases with decreasing $K$ for $K < 1$. The height of the side peaks is roughly half of the zero-bias peak in Fig. 7 due to the alignment of Fermi seas, as only one of them aligns with the dot level at finite voltage.

In this equation-of-motion approach, we ignore the contribution from higher-order correlators and thus we cannot access the Kondo regime which occurs at larger $U$. This can be seen clearly from the lack of Kondo resonance peak in the dot density of state with zero source drain voltage, or the imaginary part of the dot Green function in equilibrium. In Fig. 8, we plot the nonequilibrium steady-state dot density of state, which can be probed by placing a scanning tunneling microscope (STM) tip on top of the dot. We find, as shown in the upper inset of Fig. 8 for the $K = 0.5$ case, singular behavior at $\omega \simeq \mu_1$ or $\mu_2$ for Luttinger parameter $K$ greater than 0.26 for repulsive cases, while no singular behavior is seen for $K < 0.26$. This is similar to the situation for lifetime discussed in Fig. 6. The width of the charge resonance peaks centered around $\omega \sim \epsilon_d$ and $\epsilon_d + U$ decreases with increasing interaction strengths, while it increases with increasing source drain voltage. In the off-resonance regime where $|\omega - \epsilon_d|/(t^2 \frac{a}{\hbar v}) \gg 1$ and $|\omega - \epsilon_d - U|/(t^2 \frac{a}{\hbar v}) \gg 1$, the dot density of state goes as $|\omega|^{4\kappa-3}$ as expected from $\mathrm{Im}[G^R_d(\omega)] \sim \sum_\sigma \mathrm{Im}[\Sigma^R_\sigma(\omega)]/|\omega|^2 \propto |\omega|^{4\kappa-3}$ in the off-resonance regime.

For the interacting quantum dot system, we may tune the Luttinger parameters of the edge states to realize the transition from one-channel to two-channel Kondo physics.[14,19] The required Luttinger parameter for the repulsive case falls between 1 and 1/2 with higher-order renormalization-group analysis,[19] indicating that a weaker repulsive interaction is needed to see this transition in the Kondo regime (corresponding to $\epsilon_d + U/2 = 0$ and $\epsilon_d \to -\infty$ to suppress charge fluctuations with particle-hole symmetry in the Anderson impurity model), compared with the dot level in resonance with the equilibrium

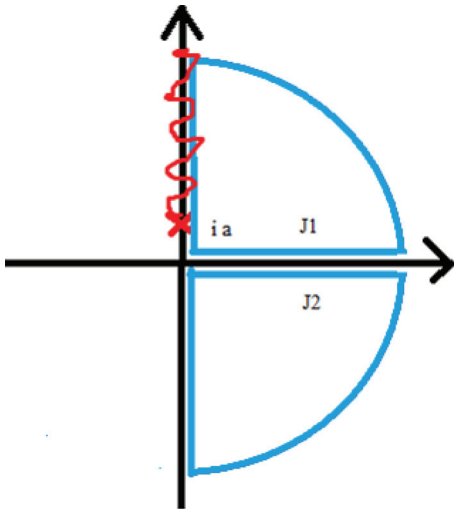


FIG. 9. (Color online) Contour chosen for evaluating $P^{++}_\alpha(\omega)$ in the complex plane. The red curvy line is the branch cut. In Eq. (A15), $J_{1\alpha}(\omega)$ is evaluated in the real axis of the upper corner and $J_{2\alpha}(\omega)$ is evaluated in the real axis of the lower corner.

Fermi surface at zero bias. This is again consistent with the results in the noninteracting dot as the physics of the one-channel to two-channel Kondo transition is closely related to the metal-to-insulating transition for this two-lead setup.

## V. CONCLUSIONS

In this paper, we consider the nonequilibrium charge current through a noninteracting or weakly interacting quantum dot connected by two helical Luttinger liquid leads. For noninteracting leads, the current is obtained by inclusion of all orders of perturbations on the Keldysh contour in the couplings between leads and dot. The interacting leads Green functions are solved by standard bosonization. We find that stronger interactions, with Luttinger parameter $K < 0.26$ in the repulsive or $K > 3.73$ in the attractive case, are required to see the metallic-to-insulating transition at zero bias when the dot level is in resonance with the equilibrium Fermi level. For the off-resonance dot level, the transition occurs at weaker interaction strengths, reaching the noninteracting limit if the dot level is far away from the zero-bias Fermi surface. This is consistent with the naive expectation, as the metal-to-insulator transition is more susceptible to the interaction of the leads if the state itself is already close to the insulating phase. Within the lowest perturbation theory with the dot in resonance with the equilibrium Fermi level, other physical quantities such as current noise, nonequilibrium lifetime, and the nonequilibrium density of state of the dot electron also show sharp to smooth transitions at $K \sim 0.26$, consistent with the scaling dimension analysis.

For a weakly interacting dot, the dot Green function is obtained perturbatively with Hartree-Fock approximations. The differential conductance is again obtained by taking a numerical derivative on the current-voltage relation. We find similar QPT as the noninteracting dot case and the charge fluctuation side peak shows similar behaviors as the zero-bias peak for the dot level in resonance with the zero-bias Fermi level. For the dot level tuned to the Kondo regime, the required

interaction strengths in the edge states to see the transition from one-channel to two-channel Kondo are weaker,[14,19] making the system ideal for observing the two-channel Kondo physics.

Finally, let us comment on the experimental feasibility of realizing this quantum phase transition and current experimental results realizing the edge-state transport of QSHI on the HgTe/CdTe quantum well devices. The rough estimate on the Luttinger parameter $K$ is given by $K^2 \sim (1+\frac{U}{2\epsilon_F})^{-1}$, where $\epsilon_F$ is the Fermi energy and $U$ is the characteristic Coulomb energy of the edge states.[36] For a HgTe/CdTe quantum well, the Coulomb energy can be controlled by the width $w$ of the well[10] (with $U \sim e^2/w$) or by placing a substrate which changes the dielectric parameters on the edge state (with $U \sim e^2/\epsilon a_0$, where $\epsilon$ is the dielectric constant). The Luttinger parameter is estimated to be $K \simeq 0.55$ for HgTe/CdTe experimental devices[4,5] and reaches $K \simeq 0.35$ for a similar device without the top gate.[7] This value is close to the large repulsive interaction strength that we need ($K \sim 0.26$) as well as the regime of $K < 1/4$ required for the "Luttinger liquid insulator" or instability threshold of the edge state.[30,31] Thus the edge-state leads are well established and fabricating a quantum dot through depositing or electron-beam lithography on the QSHI junction devices, in principle, can realize the experimental setup mentioned in this paper.

Furthermore, in Ref. 7, König *et al*. performed a spatially resolved study of backscattering in the quantum spin Hall state using scanning gate microscopy. They found that the backscattering rate at well-localized sites can be tuned by the back gate. By treating the quantum dot as an impurity site at one edge of the device, we can measure the relation between the backscattering rate and the Luttinger parameter $K$. Our results suggest that the coupling between the impurity and edge states decreases with increasing interaction strengths, which can be probed by the backscattering rate measurement. In principle, the interaction strengths of the two edges need not be the same and the $K_{cr}$ would change given this asymmetry in the real experimental setup. The qualitative features we discuss in this paper should still be valid near the metal-to-insulator transition. Note that the helical Luttinger leads need not be restricted to the quantum spin Hall system. It can also be realized in other strong spin-interaction materials, as proposed by Středa and Šeba[37] and B. Braunecker *et al*.[38]

## ACKNOWLEDGMENTS

S.-P. acknowledges useful comments from Yu-Wen Lee, Yu-Li Lee, and Thomas Schmidt, and financial support from the National Center for Theoretical Sciences in Taiwan. C.H.C. acknowledges financial support from the NSC Grant No. 101-2628-M-009-001-MY3, the MOE-ATU program, the CTS of NCTU, and the NCTS of Taiwan, Republic of China.

## APPENDIX: EVALUATION OF CORRELATION FUNCTIONS

The bare correlation function $-i\langle T_c\{\psi_{R/L\sigma}(\tau_1)\psi^\dagger_{R/L\sigma}(\tau_2)\}\rangle$ involves evaluating $-i\langle T_c\{e^{i\sqrt{4\pi}(\phi_{R/L\sigma}(\tau_1)-\phi_{R/L\sigma}(\tau'))}\eta_{R/L\sigma}(\tau_1)\eta_{R/L\sigma}(\tau_2)\}\rangle$. The bare action $S_0$ associated with helical leads Hamiltonian $H_0$ is

$$-S_0 = \int_0^\beta d\tau \int dx \Bigg( \sum_\alpha \left\{ i\nabla\Theta_\alpha(x,\tau)\partial_\tau\Phi_\alpha(x,\tau) - \frac{v_\alpha}{2}\left[K_\alpha(\nabla\Theta_\alpha)^2 + \frac{1}{K_\alpha}(\nabla\Phi_\alpha)^2\right]\right\} + \sum_\sigma d^\dagger_\sigma(\partial_\tau - \epsilon_d)d_\sigma \Bigg).$$

Here, $r^\alpha_j = (x_j, v_\alpha\tau_j)$ and we denote $\mathbf{q}_\alpha = (k, \omega_n/v_\alpha)$ as its Fourier momentum for later use. Expressing $\phi_{R\sigma} = [\Phi_c + \mathrm{sgn}(\sigma)\Phi_s - \Theta_c - \mathrm{sgn}(\sigma)\Theta_s]/2\sqrt{2}$ and $\phi_{L\sigma} = [\Phi_c + \mathrm{sgn}(\sigma)\Phi_s + \Theta_c + \mathrm{sgn}(\sigma)\Theta_s]/2\sqrt{2}$, we get the general form of the correlation function as

$$I = \left\langle T_c\left\{\prod_{\alpha,j} e^{i[A^\alpha_j\Phi_\alpha(r^\alpha_j)+B^\alpha_j\Theta_\alpha(r^\alpha_j)]}\right\}\right\rangle = e^{-\frac{1}{2}\langle T_c\{\sum_{\alpha,j}[A^\alpha_j\Phi_\alpha(r^\alpha_j)+B^\alpha_j\Theta_\alpha(r^\alpha_j)]\}^2\rangle}. \tag{A1}$$

The effect of Klein factor $-i\langle T_c\eta_{R/L\sigma}(\tau_1)\eta_{R/L\sigma}(\tau_2)\rangle$, valued at $\pm i$ depending on the ordering, will be included in the $\langle\Phi_\alpha(r^\alpha_j)\Theta_\alpha(r^\alpha_j)\rangle$ term later. The second line of Eq. (A1) has used the quadratic nature of the bosonic field $\Phi_{c,s}$ and $\Theta_{c,s}$ in the action $S_0$.

Take the Fourier component and choose $\tau_2$ on the top and $\tau_1$ on the bottom of the Keldysh contour:

$$\begin{aligned}
\langle\Phi_\alpha(r_1)\Phi_{\alpha'}(r_2)\rangle &= \frac{\delta_{\alpha,\alpha'}}{\beta\Omega}\sum_{\mathbf{q}_\alpha}\langle\Phi_\alpha(\mathbf{q}_\alpha)\Phi_\alpha(-\mathbf{q}_\alpha)\rangle e^{i\mathbf{q}_\alpha(r_1-r_2)} = \frac{\delta_{\alpha\alpha'}}{\beta}\sum_{\omega_n}\int\frac{dk}{2\pi}\frac{K_\alpha}{\omega_n^2/v_\alpha + v_\alpha k^2}e^{i(kx-\omega_n\tau)} \\
&= \delta_{\alpha\alpha'}K_\alpha\Bigg\{\int\frac{dk}{8\pi k}e^{-a_0|k|}[-f_B(-v_\alpha k)\theta(-k)e^{ikx+v_\alpha k\tau} + f_B(v_\alpha k)\theta(k)e^{ikx-v_\alpha k\tau}] + \int\frac{dk}{8\pi k}e^{-a_0|k|}[\theta(k)e^{ikx-v_\alpha k\tau} \\
&\quad - \theta(-k)e^{ikx+v_\alpha k\tau}]\Bigg\} \\
&= \delta_{\alpha\alpha'}K_\alpha\left\{\int_0^\infty\frac{dk}{4\pi k}e^{-a_0|k|}f_B(v_\alpha k)\cos(kx)e^{-v_\alpha k\tau} + \int_0^\infty\frac{dk}{4\pi k}e^{-a_0|k|}\cos(kx)e^{-v_\alpha k\tau}\right\},
\end{aligned} \tag{A2}$$

$$\langle\Theta_\alpha(r_1)\Theta_{\alpha'}(r_2)\rangle = \frac{\delta_{\alpha\alpha'}}{\beta}\sum_{\omega_n}\int\frac{dk}{2\pi}\frac{e^{i(kx-\omega_n\tau)}/K_\alpha}{\omega_n^2/v_\alpha + v_\alpha k^2} = \langle\Phi_\alpha(r_1)\Phi_{\alpha'}(r_2)\rangle/K_\alpha^2, \tag{A3}$$

$$\begin{aligned}\langle\Phi_\alpha(r_1)\Theta_{\alpha'}(r_2)\rangle &= \frac{\delta_{\alpha\alpha'}}{\beta}\sum_{\omega_n}\int\frac{dk}{2\pi}\frac{-i\omega_n e^{i(kx-\omega_n\tau)}}{k(\omega_n^2+v_\alpha^2k^2)}\\ &= \delta_{\alpha\alpha'}\left\{\int\frac{dk}{8\pi k}e^{-a_0|k|}[f_B(-v_\alpha k)\theta(-k)e^{ikx+v_\alpha k\tau}+f_B(v_\alpha k)\theta(k)e^{ikx-v_\alpha k\tau}]\right.\\ &\quad\left.+\int\frac{dk}{8\pi k}e^{-a_0|k|}[\theta(k)e^{ikx-v_\alpha k\tau}+\theta(-k)e^{ikx+v_\alpha k\tau}]\right\}\\ &= \delta_{\alpha\alpha'}\left\{\int_0^\infty\frac{dk}{4\pi k}e^{-a_0|k|}f_B(v_\alpha k)i\sin(kx)e^{-v_\alpha k\tau}+\int_0^\infty\frac{dk}{4\pi k}e^{-a_0|k|}i\sin(kx)e^{-v_\alpha k\tau}\right\}. \qquad \text{(A4)}\end{aligned}$$

Here, $f_B(x)=1/(e^{\beta x}-1)$ is the Bose-Einstein distribution function and $\beta=1/k_BT$ is the inverse temperature. At zero temperature, $f_B(x)=-\theta(-x)$. We carry out the momentum integral with $1/a_0$ as the high-energy cutoff (or, equivalently, putting in $e^{-a_0k}$ in the momentum integral) and analytically continue the imaginary time to real time component to obtain

$$\begin{aligned}\frac{1}{K_\alpha}\langle\Phi_\alpha(r_1)\Phi_{\alpha'}(r_2)\rangle &= \frac{-1}{4\pi}\ln\left[\frac{x^2+(a_0+iv_\alpha t)^2}{a_0^2}\right]\\ &\equiv F_\alpha^{(1)-+}(t,x), \qquad \text{(A5)}\\ \langle\Phi_\alpha(r_1)\Theta_{\alpha'}(r_2)\rangle &= \frac{-1}{4\pi}\ln\left[\frac{a_0+iv_\alpha t-ix}{a_0+iv_\alpha t+ix}\right]\\ &\equiv F_\alpha^{(2)-+}(t,x). \qquad \text{(A6)}\end{aligned}$$

Here, $t=t_1-t_2$ and $x=x_1-x_2$. For $t_2$ on the bottom and $t_1$ on the top branch of the Keldysh contour, we substitute $x\to-x$ and $t_1\leftrightarrow t_2$ to get

$$F_\alpha^{(1)+-}(t,x)=\frac{-1}{4\pi}\ln\left[\frac{x^2+(a_0-iv_\alpha t)^2}{a_0^2}\right], \qquad \text{(A7)}$$

$$F_\alpha^{(2)+-}(t,x)=\frac{-1}{4\pi}\ln\left[\frac{a_0-iv_\alpha t+ix}{a_0-iv_\alpha t-ix}\right]. \qquad \text{(A8)}$$

For both $t_2$ and $t_1$ on the top branch, or time-ordered branch, we get

$$\begin{aligned}F_\alpha^{(1)++}(t,x) &= \theta(t)F_\alpha^{(1)-+}(t,x)+\theta(-t)F_\alpha^{(1)+-}(t,x)\\ &= \frac{-1}{4\pi}\ln\left[\frac{x^2+(a_0+iv_\alpha|t|)^2}{a_0^2}\right], \qquad \text{(A9)}\\ F_\alpha^{(2)++}(t,x) &= \theta(t)F_\alpha^{(2)-+}(t,x)+\theta(-t)F_\alpha^{(2)+-}(t,x)\\ &= \frac{-1}{4\pi}\ln\left[\frac{a_0+iv_\alpha|t|-i\mathrm{sgn}[t]x}{a_0+iv_\alpha|t|+i\mathrm{sgn}[t]x}\right]. \qquad \text{(A10)}\end{aligned}$$

Similarly for the anti-time-ordered branch $F_\alpha^{(1)--}(t,x)$ and $F_\alpha^{(2)--}(t,x)$, obtained by $\theta(t)\leftrightarrow\theta(-t)$ in Eqs. (A9) and (A10), we get

$$F_\alpha^{(1)--}(t,x)=\frac{-1}{4\pi}\ln\left[\frac{x^2+(a_0-iv_\alpha|t|)^2}{a_0^2}\right], \qquad \text{(A11)}$$

$$F_\alpha^{(2)--}(t,x)=\frac{-1}{4\pi}\ln\left[\frac{a_0-iv_\alpha|t|+i\mathrm{sgn}[t]x}{a_0-iv_\alpha|t|-i\mathrm{sgn}[t]x}\right]. \qquad \text{(A12)}$$

We absorb the effect of Klein factor $-i\langle T_c\eta_{R/L\sigma}(\tau_1)\eta_{R/L\sigma}(\tau_2)\rangle$ by introducing $\tilde F_\alpha^{(2)++/--}(t,x)=F_\alpha^{(2)}(t,x)\pm\mathrm{sgn}[t]\frac{i}{4}$ and $\tilde F_\alpha^{(2)+-/-+}(t,x)=F_\alpha^{(2)}(t,x)\pm\frac{i}{4}$. The general form of $G_{\psi_{j,\sigma}}(\omega)$ at zero temperature is

$$\begin{aligned}G_{\psi_{j,\sigma}}(\omega) &= \int_{-\infty}^{\infty}dt e^{i(\omega-\mu_{j,\sigma})t}e^{\frac{\pi}{2}(K_c+\frac{1}{K_c})F_c^{(1)}(t,0)}\\ &\quad\times e^{\frac{\pi}{2}(K_s+\frac{1}{K_s})F_s^{(1)}(t,0)}e^{\pi[\tilde F_c^{(2)}(t,0)+\tilde F_s^{(2)}(t,0)]}. \qquad \text{(A13)}\end{aligned}$$

To compute Eq. (A13), let us first define $P_\alpha(\omega)$ as

$$\begin{aligned}\frac{1}{v_\alpha}P_\alpha\left(\frac{\omega}{v_\alpha}\right) &\equiv \frac{1}{v_\alpha}\int_{-\infty}^{\infty}dt e^{i\omega\frac{t}{v_\alpha}}e^{\pi[4\kappa_\alpha F_\alpha^{(1)}(\frac{t}{v_\alpha},0)+\tilde F_\alpha^{(2)}(\frac{t}{v_\alpha},0)]}, \qquad \text{(A14)}\\ \kappa_\alpha &\equiv \frac{1}{8}\left(K_\alpha+\frac{1}{K_\alpha}\right).\end{aligned}$$

From the above, we get the four Keldysh contour orders $P_\alpha(\frac{\omega}{v_\alpha})$ as

$$\begin{aligned}P_\alpha^{++}\left(\frac{\omega}{v_\alpha}\right) &= a_0^{2\kappa_\alpha}\int_{-\infty}^{\infty}dt\frac{e^{i\omega\frac{t}{v_\alpha}}e^{i\frac{\pi}{4}\mathrm{sgn}[t]}}{(a_0+i|t|)^{2\kappa_\alpha}},\\ P_\alpha^{--}\left(\frac{\omega}{v_\alpha}\right) &= a_0^{2\kappa_\alpha}\int_{-\infty}^{\infty}dt\frac{e^{i\omega\frac{t}{v_\alpha}}e^{-i\frac{\pi}{4}\mathrm{sgn}[t]}}{(a_0-i|t|)^{2\kappa_\alpha}},\\ P_\alpha^{+-}\left(\frac{\omega}{v_\alpha}\right) &= a_0^{2\kappa_\alpha}\int_{-\infty}^{\infty}dt\frac{e^{i\omega\frac{t}{v_\alpha}}e^{i\frac{\pi}{4}}}{(a_0-it)^{2\kappa_\alpha}},\\ P_\alpha^{-+}\left(\frac{\omega}{v_\alpha}\right) &= a_0^{2\kappa_\alpha}\int_{-\infty}^{\infty}dt\frac{e^{i\omega\frac{t}{v_\alpha}}e^{-i\frac{\pi}{4}}}{(a_0+it)^{2\kappa_\alpha}}.\end{aligned}$$

Note that $P_\alpha^{--}(\frac{\omega}{v_\alpha})=[P_\alpha^{++}(-\frac{\omega}{v_\alpha})]^*$ and $P_\alpha^{+-}(\frac{\omega}{v_\alpha})=[P_\alpha^{-+}(-\frac{\omega}{v_\alpha})]^*$ and we only need to evaluate $P_\alpha^{++}$ and $P_\alpha^{+-}$. For $P_\alpha^{++}(\omega)$ with $\omega>0$, we choose the following contour integral:

$$\begin{aligned}P_\alpha^{++}(\omega) &= a_0^{2\kappa_\alpha}\left[\int_0^\infty dt\frac{e^{i(\omega t-\frac{\pi}{4})}}{(a_0+it)^{2\kappa_\alpha}}+\int_0^\infty dt\frac{e^{i(-\omega t+\frac{\pi}{4})}}{(a_0+it)^{2\kappa_\alpha}}\right]\\ &= a_0^{2\kappa_\alpha}[J_{1\alpha}(\omega)+J_{2\alpha}(\omega)],\\ J_{1\alpha}(\omega) &= ie^{-2\pi i\kappa_\alpha}\Gamma(1-2\kappa_\alpha)\omega^{2\kappa_\alpha-1}e^{-a_0\omega-i\frac{\pi}{4}},\\ J_{2\alpha}(\omega) &= -ie^{a_0\omega}\omega^{2\kappa_\alpha-1}\Gamma(1-2\kappa_\alpha,a_0\omega)e^{i\frac{\pi}{4}}. \qquad \text{(A15)}\end{aligned}$$

Here, $\Gamma(K,z)\equiv\int_z^\infty t^{K-1}e^{-t}dt$ is the incomplete $\gamma$ function and $\Gamma(K,0)=\Gamma(K)$. For $a_0\omega\to0$ and $\omega>0$, we simplify Eq. (A15) as

$$P_\alpha^{++}(\omega)\simeq a_0^{2\kappa_\alpha}(ie^{-i(2\pi\kappa_\alpha+\frac{\pi}{4})}-ie^{i\frac{\pi}{4}})\Gamma(1-2\kappa_\alpha)\omega^{2\kappa_\alpha-1}.$$

For $\omega < 0$, we choose the left semicircle to perform the integral and we get

$$P_\alpha^{++}(\omega) \simeq a_0^{2\kappa_\alpha}(ie^{-i(2\pi\kappa_\alpha-\frac{\pi}{4})} - ie^{-i\frac{\pi}{4}})\Gamma(1-2\kappa_\alpha)(-\omega)^{2\kappa_\alpha-1}.$$

Since $P_\alpha^{++}(\omega)$ is an even function of $\omega$ and $P_\alpha^{--}(\omega) = [P_\alpha^{++}(-\omega)]^*$, we have

$$P_\alpha^{++}(\omega) \simeq a_0^{2\kappa_\alpha} i(e^{-i(2\pi\kappa_\alpha+\frac{\mathrm{sgn}(\omega)\pi}{4})} - e^{i\frac{\mathrm{sgn}(\omega)\pi}{4}})\Gamma(1-2\kappa_\alpha)|\omega|^{2\kappa_\alpha-1},$$
$$P_\alpha^{--}(\omega) \simeq -a_0^{2\kappa_\alpha} i(e^{i(2\pi\kappa_\alpha-\frac{\mathrm{sgn}(\omega)\pi}{4})} - e^{i\frac{\mathrm{sgn}(\omega)\pi}{4}})\Gamma(1-2\kappa_\alpha)|\omega|^{2\kappa_\alpha-1}.$$

For $P_\alpha^{+-}(\omega)$, we choose a different contour to perform the complex integrals and we get

$$P_\alpha^{+-}(\omega) = \Big( - ia_0^{2\kappa_\alpha} e^{i2\pi(\kappa_\alpha+\frac{1}{8})} e^{-|\omega|a_0} \int_\infty^0 dr r^{-2\kappa_\alpha} e^{-|\omega|r} + ia_0^{2\kappa_\alpha} e^{-i2\pi(\kappa_\alpha-\frac{1}{8})} e^{-|\omega|a} \int_\infty^0 dr r^{-2\kappa_\alpha} e^{-|\omega|r} \Big)\theta(-\omega)$$
$$= 2a_0^{2\kappa_\alpha} \sin(2\pi\kappa_\alpha) e^{i\frac{\pi}{4}} |\omega|^{2\kappa_\alpha-1} e^{-|\omega|a_0}\Gamma(1-2\kappa_\alpha)\theta(-\omega).$$

Thus, for $a_0\omega \to 0$, we have

$$P_\alpha^{+-}(\omega) \simeq 2\sin(2\pi\kappa_\alpha) e^{i\frac{\pi}{4}} \frac{|a_0\omega|^{2\kappa_\alpha}}{|\omega|}\Gamma(1-2\kappa_\alpha)\theta(-\omega),$$
$$P_\alpha^{-+}(\omega) \simeq 2\sin(2\pi\kappa_\alpha) e^{-i\frac{\pi}{4}} \frac{|a_0\omega|^{2\kappa_\alpha}}{|\omega|}\Gamma(1-2\kappa_\alpha)\theta(\omega).$$

Using the expressions above, we rewrite Eq. (A13) as

$$G_{\psi_{j,\sigma}}^{\mu\mu'}(\omega) = \int_{-\infty}^{\infty} \frac{dv}{2\pi v_s v_c} P_c^{\mu\mu'}\left(\frac{v}{v_c}\right) P_s^{\mu\mu'}\left(\frac{\omega-\mu_{j,\sigma}-v}{v_s}\right),$$

with $\mu$, $\mu'$ denoting $\pm$. Define $P_{\mu,\mu'}(\omega)$ as

$$P_{\mu,\mu'}(\omega) \equiv \frac{1}{v_s v_c}\int \frac{dv}{2\pi} P_c^{\mu,\mu'}\left(\frac{v}{v_c}\right) P_s^{\mu,\mu'}\left(\frac{\omega-v}{v_s}\right). \tag{A16}$$

We see that $G_{\psi_{j,\sigma}}^{\mu\mu'}(\omega) = P_{\mu,\mu'}(\omega-\mu_{j,\sigma})$. The evaluation of Eq. (A16) involves the following three integrals:

$$\int_{-\infty}^{\infty} dv|v|^{2\kappa_c-1}|\omega-v|^{2\kappa_s-1} e^{-\frac{|v|a_0}{v_c}-\frac{|\omega-v|a_0}{v_s}} \simeq \frac{\Gamma(2\kappa_c)\Gamma(2\kappa_s)}{\Gamma(2\kappa_c+2\kappa_s)} h(\kappa_c,\kappa_s)[|\omega|^{2\kappa_c+2\kappa_s-1}\theta(\omega) + |\omega|^{2\kappa_c+2\kappa_s-1}\theta(-\omega)] + O(a_0^{1-2\kappa_s-2\kappa_c}),$$
$$\int_{-\infty}^{\infty} dv|v|^{2\kappa_c-1}|\omega-v|^{2\kappa_s-1}\theta(-v)\theta(v-\omega) e^{-\frac{|v|a_0}{v_c}-\frac{|\omega-v|a_0}{v_s}} \simeq \frac{\Gamma(2\kappa_c)\Gamma(2\kappa_s)}{\Gamma(2\kappa_c+2\kappa_s)}|\omega|^{2\kappa_c+2\kappa_s-1}\theta(-\omega),$$
$$\int_{-\infty}^{\infty} dv|v|^{2\kappa_c-1}|\omega-v|^{2\kappa_s-1}\theta(v)\theta(\omega-v) e^{-\frac{|v|a_0}{v_c}-\frac{|\omega-v|a_0}{v_s}} \simeq \frac{\Gamma(2\kappa_c)\Gamma(2\kappa_s)}{\Gamma(2\kappa_c+2\kappa_s)}|\omega|^{2\kappa_c+2\kappa_s-1}\theta(\omega).$$

Here, $h(\kappa_c,\kappa_s) = 1 + \frac{\Gamma(1-2\kappa_c-2\kappa_s)\Gamma(2\kappa_c+2\kappa_s)}{\Gamma(2\kappa_c)\Gamma(1-2\kappa_c)} + \frac{\Gamma(1-2\kappa_c-2\kappa_s)\Gamma(2\kappa_c+2\kappa_s)}{\Gamma(2\kappa_s)\Gamma(1-2\kappa_s)}$. Again we have taken $a_0 \to 0$ in the computation, and the divergent terms proportional to $a_0^{1-2\kappa_s-2\kappa_c}$ for $1-2\kappa_s-2\kappa_c < 0$ in the first expression above cancel each other in the evaluation of current. Since $v_s = v_c = v$ and $K_c = 1/K_s = K$, we have $\kappa_c = \kappa_s \equiv \kappa = \frac{1}{8}(K + 1/K)$, and by collecting the above results, we get

$$G_{\psi_{j,\sigma}}^{++}(\omega) = \frac{a_0^{4\kappa}}{2\pi v^{4\kappa}}\frac{\Gamma(2\kappa)^2}{\Gamma(4\kappa)}|\omega-\mu_{j,\sigma}|^{4\kappa-1}[\tilde{h}(\kappa)\theta(\omega-\mu_{j,\sigma}) - \tilde{h}(\kappa)\theta(\mu_{j,\sigma}-\omega)],$$
$$G_{\psi_{j,\sigma}}^{--}(\omega) = \frac{a_0^{4\kappa}}{2\pi v^{4\kappa}}\frac{\Gamma(2\kappa)^2}{\Gamma(4\kappa)}|\omega-\mu_{j,\sigma}|^{4\kappa-1}[-\tilde{h}^*(\kappa)\theta(\omega-\mu_{j,\sigma}) + \tilde{h}^*(\kappa)\theta(\mu_{j,\sigma}-\omega)],$$
$$G_{\psi_{j,\sigma}}^{+-}(\omega) = \frac{2\pi a_0^{4\kappa}}{v^{4\kappa}}\frac{i}{\Gamma(4\kappa)}|\omega-\mu_{j,\sigma}|^{4\kappa-1}\theta(\mu_{j,\sigma}-\omega),$$
$$G_{\psi_{j,\sigma}}^{-+}(\omega) = \frac{2\pi a_0^{4\kappa}}{v^{4\kappa}}\frac{-i}{\Gamma(4\kappa)}|\omega-\mu_{j,\sigma}|^{4\kappa-1}\theta(\omega-\mu_{j,\sigma}), \tag{A17}$$

with $\tilde{h}(\kappa) = 2e^{-2\pi i\kappa}\sin(2\pi\kappa)\Gamma(1-2\kappa)^2$.

From Eq. (7), the current is related to the evaluation of $G_{\psi_{j,\sigma}}^{<}(\omega) = G_{\psi_{j,\sigma}}^{+-}(\omega)$, $G_{\psi_{j,\sigma}}^{A}(\omega) = G_{\psi_{j,\sigma}}^{++}(\omega) - G_{\psi_{j,\sigma}}^{-+}(\omega)$, the full retarded dot Green function $G_{d\sigma}^R(\omega) = G_{d0\sigma}^R(\omega) + G_{d0\sigma}^R(\omega)\Sigma^R(\omega)G_{d\sigma}^R(\omega)$, and the full dot lesser Green function $G_{d\sigma}^<(\omega) = G_{d\sigma}^R(\omega)\Sigma^<(\omega)G_{d\sigma}^A(\omega)$. Here the bare dot retarded Green function is $G_{d0\sigma}^R(\omega) = 1/(w-\epsilon_d+i0^+)$, and the dot self-energy is $\Sigma(\omega) \equiv \sum_{j,\sigma}|t_{j,\sigma}|^2 G_{\psi_{j,\sigma}}(\omega)$.

[1]C. L. Kane and E. J. Mele, Phys. Rev. Lett. **95**, 226801 (2005).
[2]B. A. Bernevig and S.-C. Zhang, Phys. Rev. Lett. **96**, 106802 (2006).
[3]B. A. Bernevig, T. L. Hughes, and S.-C. Zhang, Science **314**, 1757 (2006).
[4]M. König, S. Wiedmann, C. Brüne, A. Roth, H. Buhmann, L. W. Molenkamp, X.-L. Qi, and S.-C. Zhang, Science **318**, 766 (2007).
[5]C. Brüne, A. Roth, E. G. Novik, M. König, H. Buhmann, E. M. Hankiewicz, W. Hanke, J. Sinova, and L. W. Molenkamp, Nat. Phys. **6**, 448 (2010); A. Roth, C. Brüne, H. Buhmann, L. W. Molenkamp, J. Maciejko, X.-L. Qi, and S.-C. Zhang, Science **325**, 294 (2009).
[6]C. L. Kane and E. J. Mele, Phys. Rev. Lett. **95**, 146802 (2005).
[7]M. König, M. Baenninger, A. G. F. Garcia, N. Harjee, B. L. Pruitt, C. Ames, P. Leubner, C. Brüne, H. Buhmann, L. W. Molenkamp, and D. Goldhaber-Gordon, Phys. Rev. X **3**, 021003 (2013).
[8]S. Das and S. Rao, Phys. Rev. Lett. **106**, 236403 (2011).
[9]B. Braunecker, C. Bena, and P. Simon, Phys. Rev. B **85**, 035136 (2012)
[10]C.-Y. Hou, E.-A. Kim, and C. Chamon, Phys. Rev. Lett. **102**, 076602 (2009).
[11]A. Ström and H. Johannesson, Phys. Rev. Lett. **102**, 096806 (2009).
[12]J. C. Y. Teo and C. L. Kane, Phys. Rev. B **79**, 235321 (2009).
[13]C.-X. Liu, J. C. Budich, P. Recher, and B. Trauzettel, Phys. Rev. B **83**, 035407 (2011).
[14]K. T. Law, C. Y. Seng, Patrick A. Lee, and T. K. Ng, Phys. Rev. B **81**, 041305(R) (2010).
[15]C. Y. Seng and T. K. Ng, EuroPhys. Lett. **96**, 67002 (2011).
[16]T. Posske, C.-X. Liu, J. C. Budich, and B. Trauzettel, Phys. Rev. Lett. **110**, 016602 (2013).
[17]G. Dolcetto, F. Cavaliere, D. Ferraro, and M. Sassetti, Phys. Rev. B **87**, 085425 (2013).
[18]M. Fabrizio and A. O. Gogolin, Phys. Rev. B **51**, 17827 (1995).
[19]C.-H. Chung and S. Silotri, arXiv:1201.5610 (2012).
[20]C. deC. Chamon and X. G. Wen, Phys. Rev. Lett. **70**, 2605 (1993).
[21]A. Furusaki, Phys. Rev. B **57**, 7141 (1998).
[22]T. Giamarchi, *Quantum Physics in One Dimension* (Oxford University Press, Oxford, 2004).
[23]A. P. Jauho, N. S. Wingreen, and Y. Meir, Phys. Rev. B **50**, 5528 (1994).
[24]H. Haug and A.-P. Jauho, *Quantum Kinetics in Transport and Optics of Semiconductors* (Springer-Verlag, Berlin, 1998).
[25]C. L. Kane and M. P. A. Fisher, Phys. Rev. B **46**, 7268(R) (1992).
[26]C. L. Kane and M. P. A. Fisher, Phys. Rev. B **46**, 15233 (1992).
[27]T. L. Schmidt, Phys. Rev. Lett. **107**, 096602 (2011).
[28]J.-R. Souquet and P. Simon, Phys. Rev. B **86**, 161410(R) (2012).
[29]Y. W. Lee, Y. L. Lee, and C. H. Chung, Phys. Rev. B **86**, 235121 (2012).
[30]C. Wu, B. A. Bernevig, and S. C. Zhang, Phys. Rev. Lett. **96**, 106401 (2006).
[31]C. Xu and J. E. Moore, Phys. Rev. B **73**, 045322 (2006).
[32]J. Maciejko, C. Liu, Y. Oreg, X.-L. Qi, C. Wu, and S.-C. Zhang, Phys. Rev. Lett. **102**, 256803 (2009).
[33]A. O. Gogolin, A. A. Nersesyan, A. M. Tsvelik, *Bosonization and Strongly Correlated System* (Cambridge University Press, Cambridge, U.K., 2004).
[34]A. C. Hewson, *The Kondo Problem to Heavy Fermions* (Cambridge University Press, Cambridge, U.K., 1997).
[35]L. Fritz and M. Vojta, Phys. Rev. B **70**, 214427 (2004).
[36]C. L. Kane and M. P. A. Fisher, Phys. Rev. Lett. **68**, 1220 (1992).
[37]P. Středa and P. Šeba, Phys. Rev. Lett. **90**, 256601 (2003).
[38]B. Braunecker, G. I. Japaridze, J. Klinovaja, and D. Loss, Phys. Rev. B **82**, 045127 (2010).